

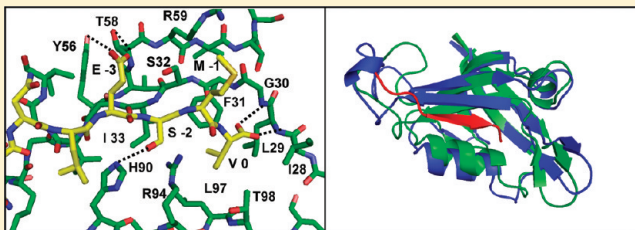
Promiscuous Binding at the Crossroads of Numerous Cancer Pathways: Insight from the Binding of Glutaminase Interacting Protein with Glutaminase L

David L. Zoetewey, Mohiuddin Ovee, Monimoy Banerjee, Rajagopalan Bhaskaran, and Smita Mohanty*

Department of Chemistry and Biochemistry, Auburn University, Auburn, Alabama 36849, United States

ABSTRACT: The glutaminase interacting protein (GIP) is composed of a single PDZ domain that interacts with a growing list of partner proteins, including glutaminase L, that are involved in a number of cell signaling and cancer pathways. Therefore, GIP makes a good target for structure-based drug design. Here, we report the solution structures of both free GIP and GIP bound to the C-terminal peptide analogue of glutaminase L. This is the first reported nuclear magnetic resonance structure of GIP in a complex with one of its binding partners.

Our analysis of both free GIP and GIP in a complex with the glutaminase L peptide provides important insights into how a promiscuous binding domain can have affinity for multiple binding partners. Through a detailed chemical shift perturbation analysis and backbone dynamics studies, we demonstrate here that the binding of the glutaminase L peptide to GIP is an allosteric event. Taken together, the insights reported here lay the groundwork for the future development of a specific inhibitor for GIP.



Protein interaction networks are essential for maintaining order and directing the flow of traffic within cells. These networks are mediated by proteins composed of one or more protein–protein interaction domains such as SH2,¹ SH3,² PH,³ PDZ,⁴ and others.⁵ PDZ domains are named for the three founding members: Post Synaptic Density 95 (PSD-95), Discs Large (Dlg), and Zonula Occludentes (ZO-1).⁶ PDZ domains are small protein–protein interaction motifs that contain 80–100 amino acid residues. They form a compact domain primarily composed of one or two α -helices and five or six β -strands. They can be found in animal species, with homologous domains also observed in yeast and plants.^{7,8} Proteins containing PDZ domains are often involved in signaling pathways and act as scaffolds in the organization of multimeric complexes, frequently in tandem with other protein–protein interaction modules.⁵ As specialized protein interaction motifs, PDZ domains are best known for binding the unstructured C-terminal tails of their binding partners. However, rarely PDZ domains can bind to internal motifs that structurally mimic a C-terminus.^{9,10} On the basis of the sequence specificity of the interacting proteins, PDZ domains are broken down into a number of different classes: class I (X-S/T-X- Φ -COOH), class II (X- Φ -X- Φ -COOH),⁵ class III (X-E/D-X- Φ -COOH),¹¹ and various other minor classes,¹² where Φ is any hydrophobic residue and X is any residue.

One such PDZ domain-containing protein that intersects a number of important biological pathways is known as either glutaminase interacting protein (GIP)¹³ or Tax interacting protein (TIP-1)¹⁴ based on the bait proteins used to find interacting partners. Human GIP is a 124-residue protein that is highly unusual among PDZ domain-containing proteins in that it is comprised almost exclusively of a single PDZ domain rather

than one of many domains as part of a larger protein.⁵ To date, GIP has been shown to interact with a number of different proteins, including glutaminase L,¹³ β -catenin,^{15,16} FAS,^{17,18} HTLV Tax,¹⁴ HPV E6,¹⁹ rhotekin,²⁰ and Kir 2.3.^{21,22} β -Catenin and rhotekin are important in the Wnt and Rho signaling pathways, respectively. FAS is a member of the tumor necrosis factor (TNF) family of receptors, while HTLV Tax and HPV E6 are both viral proteins from oncogenic viruses. Finally, the inward-rectified potassium channel Kir 2.3 is known to be regulated by GIP in renal epithelial cells. These proteins all contain the PDZ class I (X-S/T-X-I/L/V-COOH) binding motif. Thus, in addition to its regulation of glutaminase L, which has been shown to be upregulated in various cancers,^{23–25} GIP has been shown to be involved in a variety of different cancer and cell signaling pathways with its numerous binding partner proteins. Sequence alignment of all of these currently known binding partners reveals the optimal consensus sequence for GIP binding to be E-S-X-V-COOH (Table 1).

The importance of GIP as a scaffolding protein in the mammalian brain has been implicated by the demonstration of the presence of both GIP and glutaminase L in astrocytes and neurons.²⁶ Glutaminase, which is activated by inorganic phosphate, catalyzes an important energy generation reaction in mammalian tissues using glutamine as a substrate to produce glutamate and ammonia.²⁷ Glutaminase is also involved in synaptic transmission, hepatic ureagenesis, renal ammoniogenesis, and regulation of cerebral concentrations of glutamine and

Received: December 24, 2010

Revised: March 4, 2011

Published: March 18, 2011

Table 1. Sequential Alignment of C-Terminal Binding Partners of GIP

Binding Partner	Position							
	-7	-6	-5	-4	-3	-2	-1	0
Glutaminase L	K	E	N	L	E	S	M	V
Kir 2.3	S	Y	R	R	E	S	A	I
HTLV Tax	K	H	F	R	E	T	E	V
HPV E6	R	Q	A	T	E	S	T	V
Rhotekin	R	T	W	L	Q	S	P	V
β-Catenin	L	A	W	F	D	T	D	L
FAS	R	N	E	I	Q	S	L	V
Consensus	X	X	X	X	E	S	X	V

glutamate.^{13,28} There are two isoforms of the glutaminase enzyme; one is the kidney-type (K) isozyme, which is encoded by a gene located in chromosome 2, and the other is the liver-type (L) isozyme, whose coding gene locus is in chromosome 12.²⁹ Immunostaining demonstrated that glutaminase L localizes to neuronal nuclei and glutaminase K to mitochondria, suggesting a role of GIP in determining the subcellular distribution of glutaminase L as well as potential interactions with other nuclear proteins.³⁰ In both tumor cells and normally dividing cells, glutamine catabolism has been shown to be a key pathway in the process of bioenergetics.^{31–33} The C-terminus of glutaminase L has been reported to interact with several PDZ domain-containing proteins such as α-1-syntrophin (SNT) and GIP. The C-terminal end of glutaminase L contains a class I binding motif (ESMV-COOH), whereas its K counterpart lacks this motif, allowing the two isoforms to be differentially regulated and spatially localized, even when they are present in the same tissue.²⁹

Here, we report the first nuclear magnetic resonance (NMR) solution structure of a complex formed between GIP and the C-terminal peptide analogue of glutaminase L that has the sequence KENLESMV hereafter termed the glutaminase L peptide. We also demonstrate that ligand binding perturbs both NMR chemical shifts and backbone dynamics within GIP, providing important insights into the binding mechanism. The comparative structural analysis of the free and bound states of GIP provides specific knowledge about how this protein interacts with the glutaminase L peptide. Furthermore, our analysis also provides insight into the way GIP can interact with multiple different binding partners. Finally, it sets the groundwork for the design of a small molecule inhibitor for GIP that would have specificity for a number of class I PDZ domains because of their promiscuity with respect to many binding partners.

MATERIALS AND METHODS

Cloning, Overexpression, and Purification of ¹⁵N- and ¹³C-Labeled GIP. Following the procedure described previously,¹⁷ we transformed the recombinant pET-3c/GIP plasmid into *Escherichia coli* BL21(DE3)pLysS cells and expressed it in M9 minimal medium containing ¹⁵N-labeled ammonium chloride and ¹³C-labeled glucose. An overnight culture was diluted 1:25 (v/v) in minimal medium and grown at 37 °C to an OD₆₀₀ of 0.4–0.5. Expression was then induced with 1 mM IPTG at 30 °C, and after incubation for 15 h, the cells were harvested by centrifugation. The harvested cells were lysed by sonication using lysis buffer,

which contains 50 mM phosphate buffer (pH 8) as well as 200 mM NaCl, 4 mM EDTA, 4% glycerol, and 1 mM PMSF. After centrifugation of the lysed cells, the supernatant was retained for further purification. ¹⁵N- and ¹³C-labeled GIP was purified, and the NMR sample was prepared following the protocol described previously.¹⁷

Collection of NMR Data. All NMR data were collected on a Bruker Avance 600 MHz spectrometer with a triple-resonance ¹H/¹³C/¹⁵N TCI cryoprobe equipped with z-axis pulsed field gradients at either the Department of Chemistry and Biochemistry of Auburn University (Auburn, AL), Bruker BioSpin Corp. (Billerica, MA), or the New York Structural Biology Center (New York, NY). The data were processed using NMRPipe³⁴ and analyzed using NMRView³⁵ or Sparky.³⁶ For the determination of structure, samples between 500 μM and 1 mM of uniformly ¹⁵N- and ¹³C-labeled GIP in 50 mM phosphate buffer containing 5% D₂O (pH 6.5), 1 mM EDTA, and 0.01% (w/v) NaN₃ were prepared either with or without addition of the glutaminase L peptide (Chi Scientific, Maynard, MA) at a 1:3 protein:peptide ratio. All NMR experiments were performed at 298 K. To determine the ¹⁵N T₁ values, NMR spectra were recorded with relaxation delays of 10, 600, 50, 500, 100, 400, 200, 300, and 10 ms. To determine ¹⁵N T₂ values, NMR spectra were recorded with delays of 17, 153, 34, 17, 136, 51, 119, 68, 102, 85, and 34 ms. The relaxation times were randomized and some points repeated to prevent any systematic errors that may have arisen when the data were collected sequentially. The relaxation rates were calculated by least-squares fitting of peak heights versus relaxation delay to a single exponential decay. Steady-state ¹H–¹⁵N NOE values were calculated from the ratio of peak heights in a pair of NMR spectra acquired with and without proton saturation. For backbone and side chain assignments of both free GIP and the GIP–glutaminase L peptide complex, the following spectra were recorded at 298 K: two-dimensional (2D) ¹H–¹⁵N HSQC,³⁷ three-dimensional (3D) HNCACB,³⁸ 3D CC(CO)NH,³⁹ 3D CBCA(CO)NH,³⁸ 3D ¹⁵N-edited HSQC-TOCSY^{40,41} with an 80 ms mixing time, 3D HCC(CO)NH,³⁹ 3D HNHA,⁴² 3D HNCO,³⁹ and 3D HN(CA)CO.⁴³ NOE distance restraints were collected from 3D ¹⁵N-edited HSQC-NOESY^{40,41,44} and 3D ¹³C-edited HSQC-NOESY^{40,41,44} spectra with the ¹³C carrier frequency in the aliphatic (44 ppm) and aromatic (125 ppm) regions and mixing times of 140 ms for ¹⁵N and 110 ms for ¹³C. For the determination of the complex structures of GIP with the glutaminase L peptide, selectively filtered 2D NOESY⁴⁵ experiments with a mixing time of 100 ms and 3D ¹⁵N-filtered and 3D ¹³C-filtered NOESY experiments, each with mixing times of 120 ms, were performed.⁴⁶ The backbone and side chain assignments of the glutaminase L peptide were obtained with an unlabeled peptide sample (~4 mM) from the following spectra: 2D ¹H–¹⁵N HSQC, 2D ¹H–¹³C HMQC, homonuclear 2D TOCSY⁴⁷ and ROESY⁴⁸ each with a mixing time of 60 ms.

Chemical Shift Perturbation Analysis. The combined chemical shift perturbation (ΔHN) is given by the equation ΔHN = {(H_f – H_b)² + [(N_f – N_b)/10]²}^{1/2}. A scaling factor of 10 was used to normalize the differences in the ¹H and ¹⁵N spectral widths. H_f, H_b, N_f, and N_b are the chemical shifts of each residue's amide ¹H and ¹⁵N in the free (GIP alone) and bound (GIP–glutaminase L peptide complex) states, respectively. The combined chemical shift perturbation (ΔHC) is given by the equation ΔHC = {(H_f – H_b)² + [(C_f – C_b)/4]²}^{1/2}. A scaling factor of 4 was used to normalize the differences in the ¹H and ¹³C spectral widths. H_f, H_b, C_f, and C_b are the chemical shifts

Table 2. NMR Structural Statistics for the 20 Selected Lowest-Energy Structures of Free GIP and the GIP–Glutaminase L Peptide Complex

	free GIP	GIP–glutaminase L complex
no. of assignments		
sequential ($ i - j = 1$)	871	718
medium-range ($2 \leq i - j \leq 4$)	331	241
long-range ($ i - j > 4$)	622	360
intermolecular	0	37
no. of hydrogen bonds ^a	64	66
no. of dihedral constraints ^b	118	118
ensemble average ^c		
total energy	−3625 ± 125	−4816 ± 175
NOE energy	1131 ± 189	1586 ± 302
VDW energy	−937 ± 75	−1096 ± 67
bond energy	85 ± 5	170 ± 8
dihedral energy	657 ± 10	749 ± 13
angle energy	318 ± 22	434 ± 26
improper energy	963 ± 78	1009 ± 89
electrostatic energy	−4712 ± 67	−6082 ± 123
Ramachandran plot ^d		
favorable	68.6	71.2
additionally allowed	26.6	24.3
generously allowed	3.4	2.7
disallowed	1.5	1.8
rmsd (Å) ^e		
well-ordered backbone	0.45	0.67
well-ordered side chain	0.92	1.28

^a Hydrogen bonds were defined by a set of two distance restraints per bond for residues of predicted secondary structure based on TALOS⁵⁴ predictions from CSI. ^b Dihedral constraints were derived from TALOS⁵⁴ predictions from CSI. ^c Energy terms were calculated with the water refinement module of ARIA 1.2.⁵⁵ ^d Ramachandran plot statistics were calculated with PROCHECK.⁵⁶ ^e Well-ordered regions included residues 11–19, 29–36, and 54–112.

of each residue's $\alpha^1\text{H}$ and ^{13}C in the free (GIP alone) and bound (GIP–glutaminase L peptide complex) states, respectively.

Analysis of Dynamics Data. Measured relaxation parameters R_1 and R_2 and the steady-state ^1H – ^{15}N NOE for each residue were used as inputs in Modelfree version 4.15 developed by Palmer et al.^{49,50} to analyze ^{15}N backbone dynamics. The τ_c values for both free GIP and the GIP–glutaminase L peptide complex were calculated using Tensor2 for the core region of A11–Q112.^{51,52} Of five different models, the best one was chosen according to the selection criteria⁴⁹ to obtain the order parameter (S^2) that represents the degree of spatial restriction within the ^1H – ^{15}N bond vector. These values range from zero for completely isotropic internal motions to unity for totally restricted motion and represent dynamics on the picosecond to nanosecond time scale.

Structure Calculation and Refinement. A total of 4303 and 2866 NOE cross-peaks were assigned manually using Sparky³⁶ for free GIP and the GIP–glutaminase L peptide complex, respectively. The assignments were corrected or confirmed with the NOEASSIGN module of CYANA 2.1,⁵³ using the standard protocol of eight iterative cycles of NOE assignment and structure calculation. Alternately, the CANDID module of CYANA 1.0.6 was

used on the complex to initially fit the glutaminase L peptide into the binding pocket of GIP because it allowed the intermolecular assignments to be fixed separately from the intramolecular assignments. To calculate the complex structure, 36 glycine residues were added as a flexible linker between the protein and the peptide. A total of 118 dihedral angles restraints were derived from TALOS⁵⁴ based on the chemical shift index (CSI) and primary sequence of GIP for both free protein and protein–peptide complex calculations. Additionally, a total of 64 and 66 hydrogen bond distance restraints (two restraints per bond) for the free protein and the protein–peptide complex, respectively, were derived from the CSI by TALOS. During the iterative NOE assignments, a total of 1134 and 490 assignments for free GIP and the GIP–glutaminase L peptide complex were removed because of overlap, redundancy, or unresolved ambiguity that resulted from low stringency in the initial peak picking phase and high stringency in the final assignments. The final assignments averaged over 25, 18, and 12 NOEs per residue for the free protein, the protein in the complex, and the peptide in the complex, respectively. Final refinement of the 100 lowest-energy structures of the 200 total calculated structures was performed with the water refinement protocol implemented in ARIA.⁵⁵ The 20 structures with the lowest potential energy and best Ramachandran statistics as assessed by PROCHECK⁵⁶ were selected for analysis. The structures were visualized with VMD, and figures were created using Pymol.^{57,58} Table 2 shows the complete structural statistics for both structures.

RESULTS

Determination of NMR Structures of Free GIP and the GIP–Glutaminase L Peptide Complex. We have previously reported the backbone assignments of free GIP,¹⁷ which is a crucial initial rate-limiting step prior to full structural determination. Subsequently, the NMR structure of free GIP was reported by Durney et al.⁵⁹ We find good agreement between both structures of free GIP. We had previously examined the binding of several peptides representing the C-termini of various proteins, including β -catenin, FAS, and glutaminase L.¹⁷ To understand the molecular mechanism of binding of a ligand to GIP, we have initiated a detailed structural characterization of not only the free protein but also GIP in complex with its various binding partners, starting with the glutaminase L peptide. While titrating the glutaminase L peptide into GIP, we were able to track the movements of individual peaks within the ^1H – ^{15}N HSQC spectra, because most of the protein resonances are in the fast-exchange time scale. However, the peak intensities of amino acid residues I18, L21, I28–G35, Q39, D40, Q43, N44, E48, I55, E62, A66, E67, A69, and R96 either are greatly diminished or completely disappear below the noise threshold, presumably because of intermediate to slow exchange. Once GIP approaches saturation and the bound state predominates, these resonances that had disappeared earlier reappear, often in remote regions of the HSQC spectrum relative to their original positions. This caused considerable uncertainty with respect to the assignments of many of the residues predicted to be critical to complex formation, such as I28–E48 and R96, which are located within strand β_2 , the β_2 – β_3 loop, and helix α_2 . This evidence suggests that the interaction between the protein and peptide primarily proceeds through the β -strand addition mechanism⁷ rather than a direct interaction with helix α_2 . The observation of intermediate to slow exchange also suggests that there are some long-range allosteric interactions within the protein due to ligand binding, as

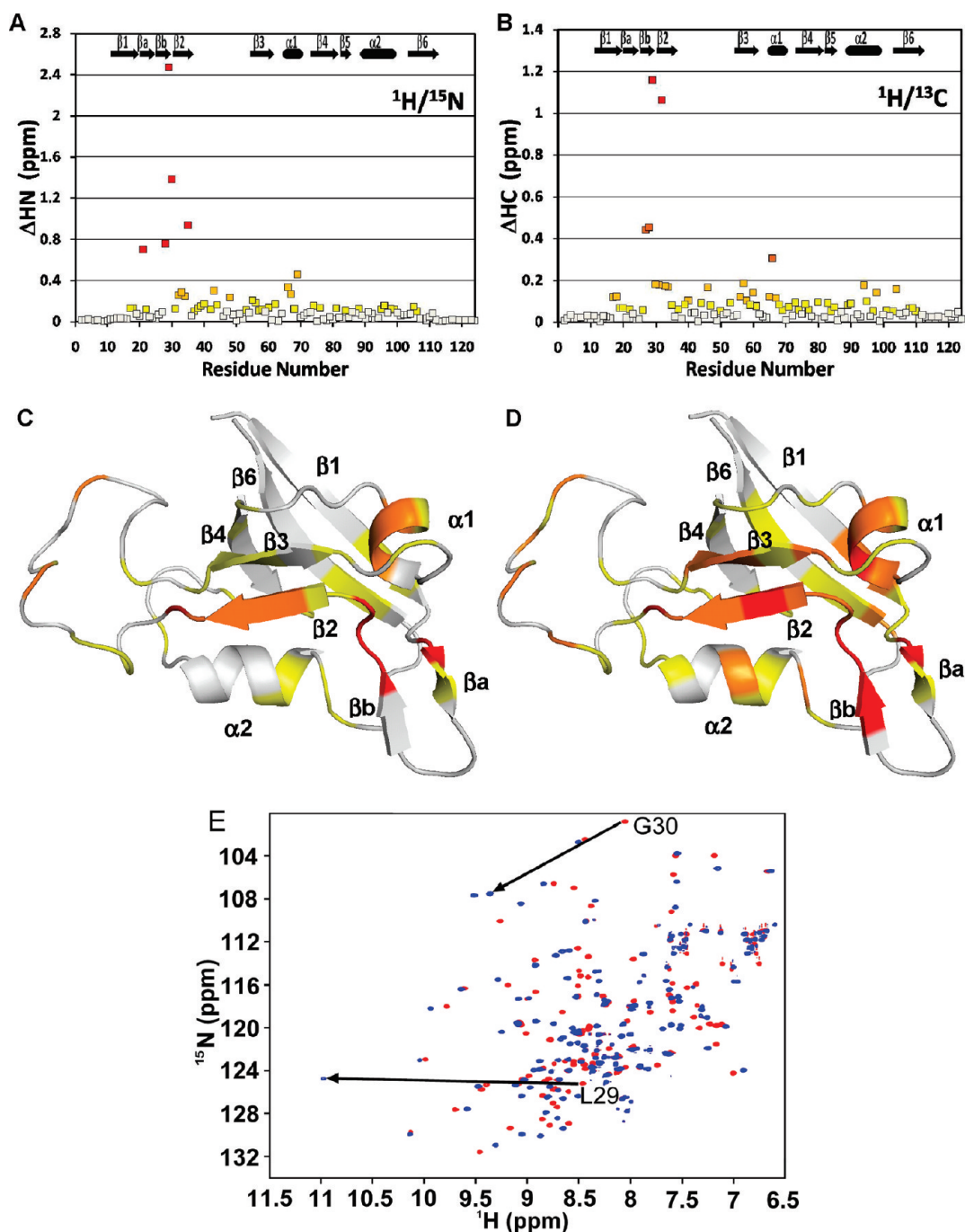


Figure 1. (A) Combined ^1H and ^{15}N backbone amide chemical shift perturbations (ΔHN) plotted as a function of residue number for GIP. (B) Combined HA and CA backbone chemical shift perturbations (ΔHC) plotted as a function of residue number for GIP. (C) Magnitudes of ΔHN presented in panel A represented in different colors on a ribbon diagram of free GIP: white for <0.1 ppm, yellow for <0.2 ppm, orange for <0.5 ppm, and red for >0.5 ppm. (D) Magnitudes of ΔHC presented in panel B represented as different colors on a ribbon diagram of free GIP: white for <0.05 ppm, yellow for <0.1 ppm, orange for <0.2 ppm, red-orange for <0.5 ppm, and red for >0.5 ppm. For panels C and D, residues A11–Q112 are shown. Residues M1–T10 and A113–S124 are not shown because they are highly disordered and have chemical shifts perturbations of <0.05 ppm. (E) Overlay of the HSQC spectra for free GIP (red) and the GIP–glutaminase L peptide complex (blue). Arrows indicate the dramatic chemical shift perturbations of L29 and G30.

this phenomenon was also seen for a number of residues that were not a direct part of the predicted binding region, such as I18, I55, and E62–A69, which belong to strands $\beta 1$ and $\beta 3$ and helix $\alpha 1$, respectively.

Likewise, the ^1H – ^{13}C HSQC spectra were remarkably different between free GIP and the GIP–glutaminase L peptide complex. Because of the severe overlap of carbon and proton

chemical shifts and the large chemical shift perturbations within GIP assignments, there was considerable uncertainty about the identity of a number of key protein side chain assignments solely on the basis of the previously assigned free GIP. Therefore, to determine the structure of the GIP–glutaminase L peptide complex, we assigned all ^{15}N , ^{13}C , and ^1H resonances from GIP in the free and complexed states using the following 3D

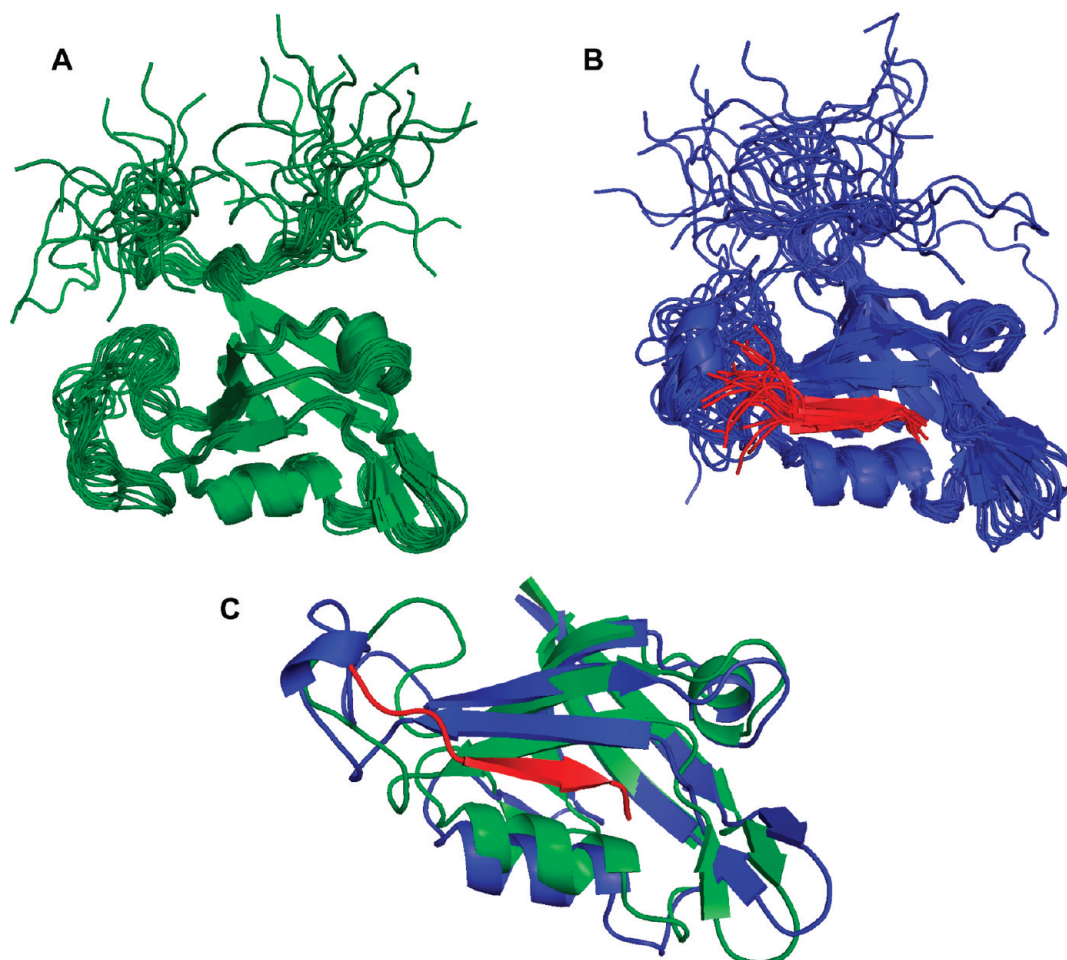


Figure 2. Ribbon diagrams of the ensemble of the 20 superimposed lowest-energy structures. (A) Free GIP is colored green. (B) Complexed GIP is colored blue and the glutaminase L peptide red. (C) Overlays of free GIP and complexed GIP are colored green and blue, respectively, with the glutaminase L peptide colored red.

experiments: HNCACB, CBCA(CO)NH, HCC(CO)NH, CC(CO)NH, HSQC-TOCSY, and HCCH-TOCSY. These experiments were used to fully reassign the protein in the complexed state, including residues, such as L27–G35, that had disappeared and reappeared in remote locations during the course of the titration of GIP with the glutaminase L peptide. The reassignment of the protein in the complex proved essential as nearly all of the resonances, both backbone and side chain, shifted either slightly or dramatically (Figure 1A,B). In general, the amide region is the most sensitive to chemical shift perturbation, but with so many overlapping ^1H and ^{13}C resonances, each assignment must be individually sorted out before structure calculation can proceed.

Determination of the NMR Structure of the GIP–Glutaminase L Peptide Complex. A number of key NMR experiments were performed with the goal of calculating the structure of the GIP–glutaminase L peptide complex. First, we used a 2D selectively filtered NOESY spectrum that can be separated into four 2D NOESY spectra.⁴⁵ This experiment selectively filters NOEs that originate from protons attached to either ^{12}C and ^{14}N (peptide) or ^{13}C and ^{15}N (protein). One of the four filtered experiments, which shows NOEs from only protons attached to ^{12}C or ^{14}N , allowed us to reassign the resonances of the glutaminase L peptide in the bound

conformation by comparing them to the resonances of the unbound form. It also helped us to determine the structure of the glutaminase L peptide in the bound state. Second, F1-filtered/F3-selected NOESY experiments with both $^{15}\text{N}/^{14}\text{N}$ and $^{13}\text{C}/^{12}\text{C}$ filtering methods were used to identify intermolecular NOEs between the unlabeled peptide and the ^{13}C - and ^{15}N -labeled protein in the complex. In addition, we identified intermolecular NOEs from the traditional 3D ^{15}N - and ^{13}C -edited NOESY experiments. Third, the selective formation of specific hydrogen bonds between the negatively charged C-terminal Val carboxyl oxygens from the glutaminase L peptide to the amide protons of L29 and G30 from GIP could be directly identified from their very large induced chemical shift perturbations.⁶⁰ These hydrogen bonds greatly enhanced the iterative assignment process in fitting the glutaminase L peptide into the structure of GIP. The GIP–glutaminase L peptide complex differs from most other complexes of PDZ domains because far fewer NOEs were observed using only the standard ^{13}C -filtered NOESY that is most frequently used to determine the structure of a complex. We believe that the lack of observable NOEs is due to line broadening resulting from intermediate to slow exchange of residues in the entire $\beta 2$ strand. Thus, only the strongest NOEs could be observed as a result of the reduced intensity of residues critical to the binding interaction. Initial

assignments of intermolecular NOEs arising from the traditional 3D (unfiltered) NOESY were ambiguous. However, once the peptide's relative position in the binding site was established, many of the initial ambiguities could be sorted out, which helped to add to the total number of intermolecular NOEs used for the final structure calculation. The ensemble of structures of both free GIP (Figure 2A) and the GIP–glutaminase L peptide complex (Figure 2B) were each calculated independently using completely different NOE data sets.

Comparison of Free GIP with the GIP–Glutaminase L Peptide Complex. In general, the architecture of a PDZ domain is characterized by a six-stranded β -roll (β 1– β 6) and two α -helices (α 1 and α 2).⁶⁰ Although there is general agreement between the structures of free GIP and the GIP–glutaminase L peptide complex, the protein does adjust to accommodate the additional β -strand in an allosteric manner. Upon binding, the α 2 helix moves away from β 2 by 0.95 Å to accommodate the additional β -strand (Figure 2C). The β 2– β 3 loop is largely unstructured in both free GIP and the complex. However, in the complex, we observe a few NOEs between this loop and the glutaminase L peptide. It has been previously reported that GIP interacts with the C-terminal β -catenin peptide through its PFS loop (residues 45–47).¹⁶ The observations mentioned above clearly demonstrate that GIP interacts with different binding partners with specificity. We observe substantial chemical shift perturbations in helix α 1 because of its relative proximity to the binding site (Figure 1). However, these chemical shift changes do not translate into the 3D structure in the complex (Figure 2). The significant chemical shift perturbations in residues not lining the binding pocket illustrate that without complete structure determination, NMR titration data can potentially be misinterpreted as an indication of direct protein–ligand interactions. It is also difficult to determine through a side-by-side structural comparison which specific interactions led to the relatively large changes in chemical shifts that we observed in regions of the protein located away from the binding site.

Glutaminase L Peptide Binding and Site Specificity. The binding pocket of GIP is formed from a groove located between helix α 2 and strand β 2. The C-terminus of the interacting protein binds to this groove as an additional antiparallel β -sheet to β 2 through β -strand addition.⁷ The sequence specificity of PDZ domains for the interacting partner is broken down into several classes usually of four residues numbered as positions –3, –2, –1, and 0 starting with the C-terminal residue as P₀. In particular, the consensus GLGF loop located at the beginning of strand β 2 forms a series of hydrogen bonds between the backbone amides of the protein and the C-terminal carboxylate of the peptide. Furthermore, this loop provides a hydrophobic pocket that helps with the sequence selectivity for the C-terminal residue of the substrate peptide.

Although both free GIP and the GIP–glutaminase L peptide complex share the same general fold typical of PDZ domains, there are several notable exceptions. Between canonical strands β 1 and β 2, GIP contains an additional short β -hairpin composed of strands β a and β b.^{16,59,61} Importantly, the final residue in strand β b is I28. Residue I28 forms the ILGF motif for GIP, which deviates from the canonical GLGF motif of PDZ domains. This suggests that while G28 is the consensus amino acid for the binding motif for PDZ domains, the mutation to Ile is tolerated perhaps because of the structural role it plays in forming the β a– β b hairpin. In contrast, G30 is the only amino acid that can accommodate the geometry needed for the formation of hydrogen

bonds from L29 and G30 of GIP to the C-terminal carboxylate of the peptide. We believe that G30 is absolutely required, as it provides a structural framework for the C-terminal specificity. In the glutaminase L peptide, the charged carboxyl group from the C-terminal Val (P₀) forms two hydrogen bonds to the backbone amide protons of L29 and G30 from GIP. Meanwhile, the hydrophobic side chain of Val (P₀) buries itself in the hydrophobic pocket created by L29, F31, L97, and I33 as well as T98 at the periphery (Figure 3). The two hydrogen bonds noted above cause unusually large chemical shift changes of up to 2.5 ppm for the amides of L29 and G30 in the ¹H–¹⁵N HSQC spectra upon binding to the peptide (Figure 1E). The chemical shift perturbations of both HN/N and HA/CA pairs show the effect of the glutaminase L peptide binding to GIP (Figure 1A,B). When these chemical shift changes are mapped onto the structure of GIP (Figure 1), one can clearly see that while regions near the binding site, including β 2, α 2, and the β 2– β 3 loop, are generally the most perturbed, α 1, which does not appear to be directly involved in the binding, is also significantly affected. This clearly demonstrates that the mechanism of binding of the peptide to GIP is allosteric. Residue H90 at the beginning of α 2 (α 2:1 in PDZ nomenclature) is oriented into the binding pocket and makes a specific hydrogen bond with the Ser at P_{–2} of the peptide (Figure 3). This is a general feature of class I PDZ domains as the residue at position α 2:1 provides the sequence selectivity that distinguishes between different classes.¹² In general, there is no specificity at P_{–1} (Table 1). The glutaminase L peptide has Met at P_{–1}, which is oriented away from the binding pocket toward the solvent. Some class I PDZ domains have specificity toward E/D or a small amino acid at P_{–3}.¹² This interaction comes from hydrogen bonds between E at P_{–3} from the glutaminase L peptide and Y56 and T58 of GIP. Alternately, a transient salt bridge could potentially exist but does not appear to be formed with R59 (Figure 3) of GIP. This particular salt bridge has been observed in the crystal structures of GIP with β -catenin¹⁶ and Kir 2.3.⁶¹ However, we did not find any observable NOEs to support the formation of a salt bridge between E at P_{–3} of the glutaminase L peptide and R59 of GIP. This is due to the dynamic flexibility of the protein side chains in solution, in contrast to the static nature of a crystal environment. It could be possible that the flexibility of these side chains would allow them to come close enough to form a transient salt bridge. However, our results demonstrate that both E at P_{–3} and R59 are solvent-exposed, thus decreasing the strength of such an interaction in solution. This demonstrates that the salt bridges observed in the two crystal structures are likely due to packing artifacts of crystallization while the true nature of the salt bridge in solution is more dynamic.

Dynamics of Free GIP and the GIP–Glutaminase L Peptide Complex from ¹⁵N Relaxation Measurements. To further elucidate the mechanism of binding of the glutaminase L peptide to GIP, we conducted backbone dynamics studies. The order parameters (*S*²) from both free and complexed forms of GIP were calculated using steady-state ¹H–¹⁵N NOE intensities and *R*₁ and *R*₂ relaxation rates using the Modelfree analysis based on the Lipari–Szabo formalism.⁶² Overlapped peaks and residues that could not be characterized because of their low intensity or absence in the HSQC spectra were excluded from our data analysis. Residues M1, P5, P8, V12, L21, P41, P45, K50, D52, P65, D75, and V80 were excluded from both free and bound states. Residues K20, L29, G30, V57, R59, I68, A69, I73, M87, K95, V105, and V118 were excluded from only the free state. Residues V13, N26, F31, G35, I37, D40, Q43, E48, D49, Y56, S61, Q72, W83, M85, T86, and A93 were excluded from only the bound state. Of these, L29, G30, F31, G35, D40, Q43, E48, and

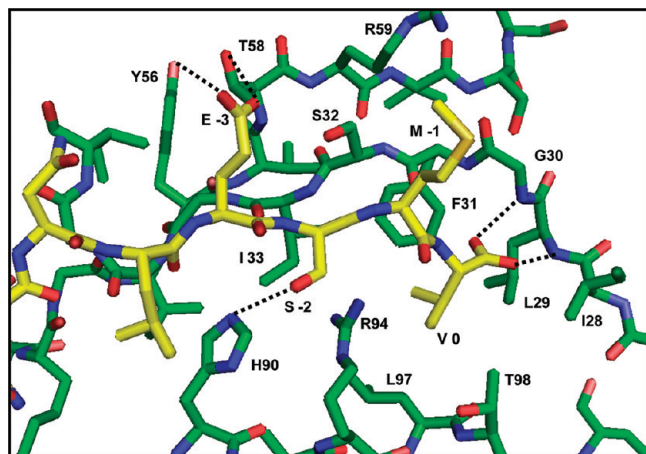


Figure 3. Close-up view of the binding site of GIP (green) with the glutaminase L peptide (yellow). Specified individual residues are labeled, and hydrogen bonds are shown as dashed lines.

D49 are residues that form part of the binding pocket, including the ILGF motif (canonical GLGF) and the $\beta 2$ – $\beta 3$ loop could not be measured. This was because they were too close to the intermediate-exchange regime to provide sufficient intensity required for observation in the NMR dynamics data. While the S^2 values could not be determined for every residue in both the free and complexed states because of either spectral overlap or line broadening, we could determine S^2 values for 100 and 96 of 118 residues (excluding the N-terminus and five prolines) for the free and bound forms of GIP, respectively. Additionally, ΔS^2 values between bound and free states were determined for 84 residues. The generalized order parameters, S^2 , are broadly similar for both the free and complexed states but exhibit certain differences as explained below. The residues located in well-defined secondary structures that exhibit relatively restricted mobilities of ≥ 0.85 are highlighted in blue (Figure 4A,C). The residues at both termini of the protein and various loops, including the βa – βb hairpin, the $\beta 2$ – $\beta 3$ loop, and a few other short loops between secondary structural elements, exhibit greater flexibility as shown in red (Figure 4A,C). We observe a correlation between our order parameters and the overall rmsd. The Modelfree analysis of free GIP yielded generally high values of S^2 with an average value of 0.89 for the core region (residues A11–Q112), indicative of the restricted backbone mobility of a well-folded protein on the subnanosecond time scale that drops off precipitously for residues at both unstructured termini (Figure 4A). Likewise, for the GIP–glutaminase L peptide complex, the average S^2 value is 0.87 for the core region. This demonstrates that in general the core of the protein maintains its structure and flexibility upon binding to the glutaminase L peptide. However, a closer examination of the changes in S^2 reveals that there are specific residues that exhibit either an increase or decrease in flexibility. For residues for which we could calculate ΔS^2 , the following showed a substantial ($\Delta S^2 > 0.06$) decrease in flexibility: G36, G54, A66, and T98 (Figure 4B). Furthermore, residues I4, T51, G74, R96, and K99 showed smaller but still significant increases in S^2 ($0.03 < \Delta S^2 < 0.06$), where the average variance in ΔS^2 was ± 0.015 for all measured residues. Twelve other residues exhibited positive but statistically insignificant increases in S^2 . Likewise, 24 residues exhibited statistically insignificant decreases in S^2 upon binding. However,

residues Q14, H19, I28, D38, N44, F46, T58, G63, G70, D91, and V109 exhibited a small but statistically significant ($-0.03 > \Delta S^2 > -0.06$) increase in flexibility. Additionally, residues R15, I18, G24, E25, L27, G34, K76, I77, H90, Q92, E103, R106, L107, and R111 and many of the measured residues in the unstructured termini (M1–T10 and S113–S124) exhibited a substantial increase in flexibility ($\Delta S^2 < -0.06$) as shown in Figure 4B. When these residues are mapped onto the structure of free GIP (Figure 4D), they demonstrate that the largest decreases in flexibility occur for residues at the C-terminal end of helix $\alpha 2$ near the binding site and at the hinge points of the $\beta 2$ – $\beta 3$ loop. However, the largest increases in backbone flexibility occur for residues located either on strands $\beta 4$ and $\beta 6$ that are distal to the binding site or in the flexible loops such as the βa – βb hairpin and the $\beta 2$ – $\beta 3$ loop.

Intermediate Exchange within GIP Caused by the Binding of the Glutaminase L Peptide. The chemical shift perturbations for most of the residues of GIP are in the fast-exchange regime as demonstrated by the titration experiments with the peptide. However, the residues lining the binding pocket appear to be in intermediate exchange. As GIP approaches saturation, residues L27, I28, L29, G30, F31, S32, I33, G34, and G35, which had disappeared or became greatly diminished because of intermediate to slow exchange at a low protein:peptide ratio, reappeared in new locations in the ^1H – ^{15}N HSQC spectra. Additionally, in the free and complexed state of GIP, residues L29 and G30 have lower intensities in the 2D ^1H – ^{15}N HSQC spectra compared to all other residues of the protein due to line broadening caused by intermediate exchange. It is noteworthy that L27–G35 are the residues that comprise the ILGF loop and most of the $\beta 2$ strand that line the binding pocket of GIP. Along with significant chemical shift perturbations, there are substantial changes in the measurable order parameters for different regions within the binding pocket. It appears that both ends of the binding pocket experience opposite effects on its S^2 values. One end of the binding pocket that is near the C-terminus of the peptide is composed of the ILGF loop and the C-terminal half of helix $\alpha 2$ (K95–R100). Residues L29, G30, and F31 of the ILGF loop are in intermediate exchange, which precludes the measurement of ΔS^2 . Residues R96, T98, and K99 from helix $\alpha 2$ experience a decrease in flexibility upon binding the C-terminal end of the peptide. However, at the opposite end of the binding pocket, residues from both $\beta 2$ and $\alpha 2$ (G34, H90, and Q92) experience an increase in flexibility. This is reflected in the relatively high rmsd for the N-terminal end of the glutaminase L peptide. This observation of increased or decreased flexibility in the binding pocket of the protein and that of the peptide suggests that the substrate specificity is limited to the four C-terminal residues of glutaminase L.

DISCUSSION

Binding Specificity of the Glutaminase L Peptide with GIP.

The specificity of GIP toward the target protein C-terminal sequence, i.e., E-S/T-X-I/L/V-COOH (Table 1), of the glutaminase L peptide comes from various interactions. The amide protons of residues L29 and G30 in the ILGF loop are uniquely positioned in a way that allows them to form a pair of hydrogen bonds to both carboxyl oxygen atoms of V at P₀ from the glutaminase L peptide (Figure 3). These interactions are characterized by the very large chemical shift perturbations observed for the L29 and G30 amide groups (Figure 1A,E). Although the

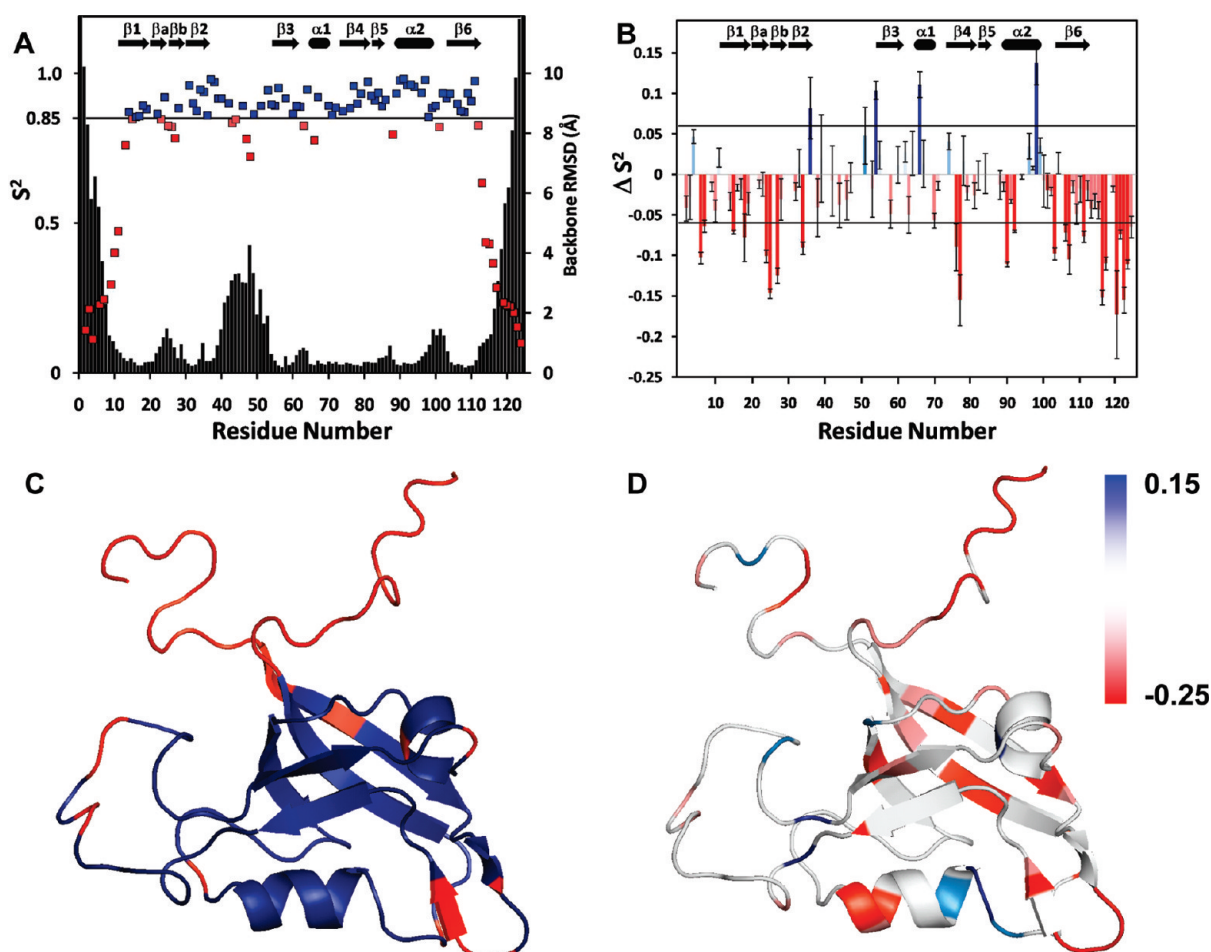


Figure 4. (A) S^2 values derived using the Modelfree analysis from the steady-state ^1H – ^{15}N NOE and R_1 and R_2 relaxation times of free GIP for each nonoverlapping well-defined residue. Residues with order parameters above the threshold of 0.85 are colored blue while those with values below red. The backbone rmsd of free GIP for each residue is overlaid on this plot in black. (B) Plot of ΔS^2 as a function of residue number, where ΔS^2 refers to the S^2 of the GIP–glutaminase L peptide complex minus that of free GIP. Positive values are indicated with increasing blue intensity, while negative values are indicated with increasing red intensity. (C) Residues with S^2 values below the threshold of 0.85 are mapped in red onto the structure of free GIP colored blue. (D) Magnitude of ΔS^2 upon binding to the glutaminase L peptide mapped onto the structure of free GIP and indicated by the darker intensity for red (increased flexibility) or blue (decreased flexibility). Residues were colored white for one of the following reasons: they could not be measured in both structures because of overlap, they had ΔS^2 values between the threshold values of 0.06 and -0.06 , or the residue was a proline.

structure is not significantly affected, the chemical environment is dramatically different because of the proximity to the negatively charged carboxyl oxygens from the C-terminus of the peptide. The peptide binding also dramatically affects the dynamics of GIP, so much so that residues L27–G35 disappear during the course of the titration into the intermediate- to slow-exchange regime and do not reappear until after the binding site becomes saturated.

The specificity for a hydrophobic residue at P_0 comes from the hydrophobic pocket created by L29, F31, I33, and L97. Val seems to be preferred at P_0 more than Leu or Ile. The steric nature of these hydrophobic interactions can be investigated through point mutation of one or more of the following residues in the binding pocket of GIP: L29V, L97V, or T98A. Residue L97, located at position $\alpha 2:8$, is highly conserved across class I PDZ domains and is known to confer specificity at P_0 .¹² The side chains of L29 and L97 interact to form the majority of the surface area of this hydrophobic pocket. These mutations would likely change the selectivity at P_0 from Val to Ile, Leu, or a potentially larger hydrophobic amino acid currently not allowed such as Phe or Trp.

Specificity for S or T at P_{-2} is due to H90 at position $\alpha 2:1$ of GIP. In contrast, the reasons for the lack of specificity at P_{-1} appear to be 2-fold. Residue G30 is highly conserved across PDZ domains. The geometry of G30 is a steric requirement for the binding to the C-terminus of the target protein. The absence of a side chain at this position most likely serves as an evolutionary trade-off between specificity for the C-terminus and sequence specificity at P_{-1} . Second, because the binding occurs as β -strand addition, alternating amino acids are oriented away from the binding site.

By comparing the first NMR structure of the GIP–glutaminase L peptide complex to the crystal structures of GIP bound to other target proteins, we can identify and distinguish between common and unique features of binding for each ligand. We have shown here that the mode of binding between GIP and each of its ligands is unique and specific. We show that only a few interactions occur between the $\beta 2$ – $\beta 3$ loop of GIP and the glutaminase L peptide, unlike the specific interactions seen between the PFS loop of GIP and β -catenin.¹⁶ Additionally, the E at P_{-3} of the glutaminase L peptide makes specific hydrogen bonds to Y56 and

T58 of GIP rather than the salt bridge observed between the D or E at P₋₃ of β -catenin or Kir 2.3 and R59 of GIP that we believe to be crystallization artifacts.^{16,61} In comparison to the observed changes in chemical shifts for other ligands of GIP such as β -catenin and FAS that we have previously reported,¹⁷ the unique mode of binding and chemical shift perturbation patterns observed for GIP with the glutaminase L peptide means that it is necessary to experimentally determine the structure of GIP in complex with each of its known ligands.

By maximizing the common features and taking advantage of the unique features of ligand binding, we should be able to efficiently design a competitive inhibitor with an affinity higher than that of any of the natural ligands. In the design of a target site inhibitor, a good choice at P₋₁ would likely be a hydrophilic and specifically negatively charged residue such as D or E to potentially form a salt bridge with R59¹⁶ rather than hydrophobic because it is solvent-exposed. Specificity for E at P₋₃ of the peptide is due to the formation of a hydrogen bond with Y56 and/or T58 of GIP. Because Y56 and T58 can each act as hydrogen bond donors or acceptors, this explains why P₋₃ can also accommodate multiple side chains. Furthermore, GIP has three glycines in a row: G34, G35, and G36. The lack of side chains for these residues can explain the binding of GIP to various binding partners. Finally, GIP has specificity for β -catenin that is not present for the glutaminase L peptide, at positions beyond P₋₃. An aromatic residue at P₋₅ or P₋₆ (Table 1) could provide additional specificity for GIP for any future drug design effort.

Effects of Binding of the Glutaminase L Peptide on the Dynamics of GIP. Where S^2 could be measured in both free GIP and the GIP–glutaminase L complex, some residues show either substantial increases or decreases in backbone flexibility. In general, residues at the binding site tend to become more ordered, while residues peripheral to the binding site in GIP become more disordered, with a few exceptions. G34 is part of the β_2 strand that forms an antiparallel β -sheet with the glutaminase L peptide and thus should be more stabilized, yet it actually becomes more disordered. While it is part of the binding site, it is located on the opposite end of strand β_2 from the ILGF binding loop and is near the hinge point between strand β_2 and the β_2 – β_3 loop (residues G36–G54). Additionally, H90, D91, and Q92 exhibit increased flexibility. While H90 makes a direct hydrogen bond to the S at P₋₂ (Figure 3), the specificity of the glutaminase L peptide is limited to the four C-terminal residues, while the N-terminal four residues are disordered with higher rmsd values. However, the general trend is that in the regions of GIP where the peptide directly interacts, the structure becomes more rigid, which is offset by an increase in flexibility that is distributed throughout the rest of the protein. The decrease in the flexibility of the binding pocket is offset by an increase in flexibility distal to the binding site in the core of the protein, including strands β_1 , β_4 , and β_6 . Furthermore, the increase in flexibility throughout GIP also includes the flexible regions of the protein such as the β_a – β_b hairpin and β_2 – β_3 loops as well as both termini.

Comparison to Other GIP Complexes. It is worth noting that both the N-terminal (M1–T10) and C-terminal (S113–S124) regions of GIP are completely unstructured both in the free state and in the complex with very few observed NOEs and correspondingly high rmsds in our structural ensembles (Figure 2A,B). This is further supported by our dynamics data, which also show these regions to be completely unstructured (Figure 4A). It has

been previously reported that C-terminal truncation of GIP leads to a decreased affinity for full length β -catenin *in vivo*.¹⁵ We observed general similarity in the modes of binding of the β -catenin and glutaminase L peptides to GIP.¹⁷ Therefore, it appears unlikely that the reported decrease in the affinity of full-length β -catenin for a C-terminally truncated GIP is due to an interaction between the canonical C-terminal binding motif of β -catenin and the C-terminus (residues 113–124) of GIP. We previously observed very little change in the chemical shifts of the C-terminal region of GIP upon ligand binding, regardless of whether the ligand is the glutaminase L, β -catenin, or FAS peptide.¹⁷ Therefore, we propose a possible explanation for the observed decrease in the affinity for the full-length β -catenin upon C-terminal truncation of GIP. The C-terminus of GIP most likely interacts with either a different region of full-length β -catenin or another interacting partner protein *in vivo*. This hypothesis is supported by the *in vivo* two-hybrid interaction studies between various deletion mutants for both GIP and β -catenin.¹⁵ These studies showed a central core region of β -catenin (residues 173–483) lacking the class I C-terminal motif still maintained some affinity for GIP.¹⁵ We believe that the best explanation of these results, in light of our structural and dynamics characterization, is that it is the central core region of β -catenin that interacts directly and specifically with the C-terminus of GIP. Taken together, it appears that β -catenin and GIP each bind to the other protein's C-terminus.

Comparison of NMR and Crystal Structures of Free GIP. A solution NMR structure provides insight into the dynamic nature of a protein. By comparing the solution structure of free GIP with the previously determined crystal structures, we show that while there is good agreement between NMR and crystallographic methods, there are a few key differences. First, in each of the NMR structures, both the N- and C-termini (residues 1–10 and 113–124, respectively) are highly dynamic and unstructured. This is in contrast to the crystal structure of free GIP where the C-terminus forms a helix, which is most likely an artifact of crystallization. Second, the β_2 – β_3 loop from G36 to G54 has a defined structure in the crystal structures,^{16,61} but it is considerably more flexible in our NMR structure. Our dynamics data also indicate that this region had significantly lower order parameters compared to the rest of the central core region. Additionally, relatively few NOEs were observed compared to other regions of the protein. All of the observed NOEs were medium-range ($|i - j| < 5$) or shorter, but there were no unambiguously defined long-range NOEs ($|i - j| > 5$). We found this to be the case for both free GIP and the GIP–glutaminase L peptide complex. However, there were some intermolecular NOEs between the loop and the peptide, which indicates that this flexible loop may undergo a conformational change upon binding. This conformational change is observed from the decrease in the flexibility of G36 and G54 near the hinge point of the β_2 – β_3 loop while flexibility increases on either side of the hinge point. We do observe a distinct conformational change (Figure 2C), but the loop remains relatively unstructured compared to the rest of the core protein in both free and bound states. Third, the noncanonical β -hairpin formed by residues L21–I28 has a higher relative backbone rmsd of ~ 0.85 Å in the free form of GIP compared to the rest of the core structured portion of the protein at 0.45 Å. In the GIP–glutaminase L complex, the corresponding rmsd values are 2.73 and 0.67 Å, respectively. As was the case for the β_2 – β_3 loop, there are NOEs that define the β -hairpin. However, because it is exposed to the solvent, it does not make as many

contacts with the rest of the protein and is therefore relatively unconstrained during the structural calculation. The increase in rmsd for this hairpin loop within the complex is due to relatively fewer long-range NOEs observed for the GIP–glutaminase L peptide complex than for free GIP. It is further supported by the increases in flexibility for the complex seen for residues G24, E25, L27, and I28.

Potential for Targeted Drug Design. Taken together, the elements of specificity within GIP for certain types of molecular interactions do make it a tempting target for drug design. Because cells contain literally hundreds of PDZ domains, a potential drug would have to be designed to interact very specifically with only the PDZ domain within GIP or to broadly target and disrupt the function of other PDZ domains that may share the same specificity as GIP. The structural insights provided by the GIP–glutaminase L peptide complex in this study can form the basis for the development of promising anticancer therapeutics targeting GIP.

Accession Codes

The chemical shifts of the resonances and the atomic coordinates for free GIP as well as the GIP–glutaminase L peptide complex have been deposited in the BioMagnetic Resonance Bank (BMRB) and the Protein Data Bank (PDB) with the following accession numbers: 17254 and 17255 for the BMRB and 2L4S and 2L4T for the PDB, respectively.

AUTHOR INFORMATION

Corresponding Author

*E-mail: mohansm@auburn.edu. Phone: (334) 844-7081. Fax: (334) 844-6959. Address: 266 Chemistry Building, Auburn, AL 36849.

Author Contributions

D.L.Z. and M.O. made equal contributions to this work.

Funding Sources

This research was financially supported by U.S. Department of Agriculture PECASE Presidential Early Career Award for Scientists and Engineers Award 2003-35302-12930, National Science Foundation Grant IBN-0628064, and National Institutes of Health Grant DK082397 to S.M.

ACKNOWLEDGMENT

We thank Dr. Donna M. Baldisseri of the Bruker BioSpin Corp. (Billerica, MA) for some of the NMR data collection as well as Dr. Uma Katre and Dr. Janarthanan Krishnamoorthy for help with figure preparation and Prof. Peter Livant (Department of Chemistry and Biochemistry, Auburn University) for critical reading of the manuscript.

DEDICATION

The authors dedicate this article in the loving memory of Dr. Marie W. Wooten, Dean and Professor of the College of Sciences and Mathematics (COSAM) at Auburn University, who tragically passed away on November 5, 2010. Dean Wooten was our mentor, colleague, friend, and role model. She will be deeply and painfully missed, yet celebrated, honored, and never forgotten.

ABBREVIATIONS

NMR, nuclear magnetic resonance; PDZ, Post Synaptic Density 95, Discs Large, Zonula Occludentes 1; GIP, glutaminase interacting protein; NOE, nuclear Overhauser effect; rmsd, root-mean-square deviation.

REFERENCES

- (1) Neel, B. G. (1993) Structure and function of SH2-domain containing tyrosine phosphatases. *Semin. Cell Biol.* 4, 419–432.
- (2) Kardinal, C., Posern, G., Zheng, J., Knudsen, B. S., Moarefi, I., and Feller, S. M. (1999) Rational development of cell-penetrating high affinity SH3 domain binding peptides that selectively disrupt the signal transduction of Crk family adapters. Amgen Peptide Technology Group. *Ann. N.Y. Acad. Sci.* 886, 289–292.
- (3) Falke, J. J. (2007) Membrane Recruitment as a Cancer Mechanism: A Case Study of Akt PH Domain. *Cell Sci.* 4, 25–30.
- (4) Fanning, A. S., and Anderson, J. M. (1996) Protein-protein interactions: PDZ domain networks. *Curr. Biol.* 6, 1385–1388.
- (5) Garcia-Mata, R., and Burridge, K. (2007) Catching a GEF by its tail. *Trends Cell Biol.* 17, 36–43.
- (6) Woods, D. F., and Bryant, P. J. (1993) ZO-1, DlgA and PSD-95/SAP90: Homologous proteins in tight, septate and synaptic cell junctions. *Mech. Dev.* 44, 85–89.
- (7) Jelen, F., Oleksy, A., Smietana, K., and Otlewski, J. (2003) PDZ domains: Common players in the cell signaling. *Acta Biochim. Pol.* 50, 985–1017.
- (8) Spaller, M. R. (2006) Act globally, think locally: Systems biology addresses the PDZ domain. *ACS Chem. Biol.* 1, 207–210.
- (9) Christopherson, K. S., Hillier, B. J., Lim, W. A., and Bredt, D. S. (1999) PSD-95 assembles a ternary complex with the N-methyl-D-aspartic acid receptor and a bivalent neuronal NO synthase PDZ domain. *J. Biol. Chem.* 274, 27467–27473.
- (10) Lemaire, J. F., and McPherson, P. S. (2006) Binding of Vac14 to neuronal nitric oxide synthase: Characterisation of a new internal PDZ-recognition motif. *FEBS Lett.* 580, 6948–6954.
- (11) Wiedemann, U., Boisguerin, P., Leben, R., Leitner, D., Krause, G., Moelling, K., Volkmer-Engert, R., and Oschkinat, H. (2004) Quantification of PDZ domain specificity, prediction of ligand affinity and rational design of super-binding peptides. *J. Mol. Biol.* 343, 703–718.
- (12) Tonikian, R., Zhang, Y., Sazinsky, S. L., Currell, B., Yeh, J. H., Reva, B., Held, H. A., Appleton, B. A., Evangelista, M., Wu, Y., Xin, X., Chan, A. C., Seshagiri, S., Lasky, L. A., Sander, C., Boone, C., Bader, G. D., and Sidhu, S. S. (2008) A specificity map for the PDZ domain family. *PLoS Biol.* 6, e239.
- (13) Olalla, L., Aledo, J. C., Bannenberg, G., and Marquez, J. (2001) The C-terminus of human glutaminase L mediates association with PDZ domain-containing proteins. *FEBS Lett.* 488, 116–122.
- (14) Rousset, R., Fabre, S., Desbois, C., Bantignies, F., and Jalinot, P. (1998) The C-terminus of the HTLV-1 Tax oncoprotein mediates interaction with the PDZ domain of cellular proteins. *Oncogene* 16, 643–654.
- (15) Kanamori, M., Sandy, P., Marzinotto, S., Benetti, R., Kai, C., Hayashizaki, Y., Schneider, C., and Suzuki, H. (2003) The PDZ protein tax-interacting protein-1 inhibits β -catenin transcriptional activity and growth of colorectal cancer cells. *J. Biol. Chem.* 278, 38758–38764.
- (16) Zhang, J., Yan, X., Shi, C., Yang, X., Guo, Y., Tian, C., Long, J., and Shen, Y. (2008) Structural basis of β -catenin recognition by Tax-interacting protein-1. *J. Mol. Biol.* 384, 255–263.
- (17) Banerjee, M., Huang, C., Marquez, J., and Mohanty, S. (2008) Probing the structure and function of human glutaminase-interacting protein: A possible target for drug design. *Biochemistry* 47, 9208–9219.
- (18) Saras, J., Engstrom, U., Gonce, L. J., and Heldin, C. H. (1997) Characterization of the interactions between PDZ domains of the protein-tyrosine phosphatase PTP1L and the carboxyl-terminal tail of Fas. *J. Biol. Chem.* 272, 20979–20981.

- (19) Hampson, L., Li, C., Oliver, A. W., Kitchener, H. C., and Hampson, I. N. (2004) The PDZ protein Tip-1 is a gain of function target of the HPV16 E6 oncoprotein. *Int. J. Oncol.* 25, 1249–1256.
- (20) Reynaud, C., Fabre, S., and Jalinot, P. (2000) The PDZ protein TIP-1 interacts with the Rho effector rhotekin and is involved in Rho signaling to the serum response element. *J. Biol. Chem.* 275, 33962–33968.
- (21) Le Maout, S., Welling, P. A., Brejon, M., Olsen, O., and Merot, J. (2001) Basolateral membrane expression of a K⁺ channel, Kir 2.3, is directed by a cytoplasmic COOH-terminal domain. *Proc. Natl. Acad. Sci. U.S.A.* 98, 10475–10480.
- (22) Alewine, C., Olsen, O., Wade, J. B., and Welling, P. A. (2006) TIP-1 has PDZ scaffold antagonist activity. *Mol. Biol. Cell* 17, 4200–4211.
- (23) Perez-Gomez, C., Campos-Sandoval, J. A., Alonso, F. J., Segura, J. A., Manzanera, E., Ruiz-Sanchez, P., Gonzalez, M. E., Marquez, J., and Mates, J. M. (2005) Co-expression of glutaminase K and L isoenzymes in human tumour cells. *Biochem. J.* 386, 535–542.
- (24) Gao, P., Tchernyshyov, I., Chang, T. C., Lee, Y. S., Kita, K., Ochi, T., Zeller, K. I., De Marzo, A. M., Van Eyk, J. E., Mendell, J. T., and Dang, C. V. (2009) c-Myc suppression of miR-23a/b enhances mitochondrial glutaminase expression and glutamine metabolism. *Nature* 458, 762–765.
- (25) Gallagher, F. A., Kettunen, M. I., Day, S. E., Lerche, M., and Brindle, K. M. (2008) ¹³C MR spectroscopy measurements of glutaminase activity in human hepatocellular carcinoma cells using hyperpolarized ¹³C-labeled glutamine. *Magn. Reson. Med.* 60, 253–257.
- (26) Olalla, L., Gutierrez, A., Jimenez, A. J., Lopez-Tellez, J. F., Khan, Z. U., Perez, J., Alonso, F. J., de la Rosa, V., Campos-Sandoval, J. A., Segura, J. A., Aledo, J. C., and Marquez, J. (2008) Expression of the scaffolding PDZ protein glutaminase-interacting protein in mammalian brain. *J. Neurosci. Res.* 86, 281–292.
- (27) Krebs, H. A. (1935) Metabolism of amino-acids: The synthesis of glutamine from glutamic acid and ammonia, and the enzymic hydrolysis of glutamine in animal tissues. *Biochem. J.* 29, 1951–1969.
- (28) Curthoys, N. P., and Watford, M. (1995) Regulation of glutaminase activity and glutamine metabolism. *Annu. Rev. Nutr.* 15, 133–159.
- (29) Aledo, J. C., Gomez-Fabre, P. M., Olalla, L., and Marquez, J. (2000) Identification of two human glutaminase loci and tissue-specific expression of the two related genes. *Mamm. Genome* 11, 1107–1110.
- (30) Olalla, L., Gutierrez, A., Campos, J. A., Khan, Z. U., Alonso, F. J., Segura, J. A., Marquez, J., and Aledo, J. C. (2002) Nuclear localization of L-type glutaminase in mammalian brain. *J. Biol. Chem.* 277, 38939–38944.
- (31) Medina, M. A., Sanchez-Jimenez, F., Marquez, J., Rodriguez Quesada, A., and Nunez de Castro, I. (1992) Relevance of glutamine metabolism to tumor cell growth. *Mol. Cell. Biochem.* 113, 1–15.
- (32) Brand, K. (1985) Glutamine and glucose metabolism during thymocyte proliferation. Pathways of glutamine and glutamate metabolism. *Biochem. J.* 228, 353–361.
- (33) Kovacevic, Z., and McGivan, J. D. (1983) Mitochondrial metabolism of glutamine and glutamate and its physiological significance. *Physiol. Rev.* 63, 547–605.
- (34) Delaglio, F., Grzesiek, S., Vuister, G. W., Zhu, G., Pfeifer, J., and Bax, A. (1995) NMRPipe: A multidimensional spectral processing system based on UNIX pipes. *J. Biomol. NMR* 6, 277–293.
- (35) Johnson, B. A. (2004) Using NMRView to visualize and analyze the NMR spectra of macromolecules. *Methods Mol. Biol.* 278, 313–352.
- (36) Goddard, T. D., and Kneller, D. G. (2008) SPARKY 3, University of California, San Francisco.
- (37) Kay, L., Keifer, P., and Saarinen, T. (1992) Pure absorption gradient enhanced heteronuclear single quantum correlation spectroscopy with improved sensitivity. *J. Am. Chem. Soc.* 114, 10663–10665.
- (38) Muhandiram, D. R., and Kay, L. E. (1994) Gradient-Enhanced Triple-Resonance Three-Dimensional NMR Experiments with Improved Sensitivity. *J. Magn. Reson., Ser. B* 103, 203–216.
- (39) Grzesiek, S., and Bax, A. (1992) Correlating backbone amide and side chain resonances in larger proteins by multiple relayed triple resonance NMR. *J. Am. Chem. Soc.* 114, 6291–6293.
- (40) Norwood, T. J., Boyd, J., Heritage, J. E., Soffe, N., and Campbell, I. D. (1990) Comparison of techniques for ¹H-detected heteronuclear ¹H–¹⁵N Spectroscopy. *J. Magn. Reson.* 87, 488–501.
- (41) Palmer, A. G., Cavanagh, J., Wright, P. E., and Rance, M. (1991) Sensitivity improvement in proton-detected two-dimensional heteronuclear correlation NMR spectroscopy. *J. Magn. Reson.* 93, 151–170.
- (42) Vuister, G. W., and Bax, A. (1993) Quantitative J correlation: A new approach for measuring homonuclear three-bond J_{HNHα} coupling constants in ¹⁵N-enriched proteins. *J. Am. Chem. Soc.* 115, 7772–7777.
- (43) Clubb, R. T., Thanabal, V., and Wagner, G. (1992) A constant-time three-dimensional triple-resonance pulse scheme to correlate intrasidue ¹HN, ¹⁵N, and ¹³C' chemical shifts in ¹⁵N–¹³C-labelled proteins. *J. Magn. Reson.* 97, 213–217.
- (44) Zhang, O., Kay, L. E., Olivier, J. P., and Forman-Kay, J. D. (1994) Backbone ¹H and ¹⁵N resonance assignments of the N-terminal SH3 domain of drk in folded and unfolded states using enhanced-sensitivity pulsed field gradient NMR techniques. *J. Biomol. NMR* 4, 845–858.
- (45) Otting, G., and Wüthrich, K. (1989) Extended heteronuclear editing of 2D ¹H NMR spectra of isotope-labeled proteins, using the X(ω₁, ω₂) double half filter. *J. Magn. Reson.* 85, 586–594.
- (46) Zwaalen, C., Legault, P., Vincent, S. J. F., Greenblatt, J., Konrat, R., and Kay, L. E. (1997) Methods for Measurement of Intermolecular NOEs by Multinuclear NMR Spectroscopy: Application to a Bacteriophage λ N-Peptide/boxB RNA Complex. *J. Am. Chem. Soc.* 119, 6711–6721.
- (47) Bax, A., and Davis, D. G. (1985) MLEV-17-based two-dimensional homonuclear magnetization transfer spectroscopy. *J. Magn. Reson.* 65, 355–360.
- (48) Bax, A., and Davis, D. G. (1985) Practical aspects of two-dimensional transverse NOE spectroscopy. *J. Magn. Reson.* 63, 207–213.
- (49) Mandel, A. M., Akke, M., and Palmer, A. G., III (1995) Backbone dynamics of *Escherichia coli* ribonuclease HI: Correlations with structure and function in an active enzyme. *J. Mol. Biol.* 246, 144–163.
- (50) Palmer, A. G., Rance, M., and Wright, P. E. (1991) Intramolecular motions of a zinc finger DNA-binding domain from Xfin characterized by proton-detected natural abundance carbon-13 heteronuclear NMR spectroscopy. *J. Am. Chem. Soc.* 113, 4371–4380.
- (51) Dosset, P., Hus, J.-C., Blackledge, M., and Marion, D. (2000) Efficient analysis of macromolecular rotational diffusion from heteronuclear relaxation data. *J. Biomol. NMR* 16, 23–28.
- (52) Tsan, P., Hus, J.-C., Caffrey, M., Marion, D., and Blackledge, M. (2000) Rotational Diffusion Anisotropy and Local Backbone Dynamics of Carbon Monoxide-Bound *Rhodobacter capsulatus* Cytochrome c'. *J. Am. Chem. Soc.* 122, 5603–5612.
- (53) Guntert, P. (2004) Automated NMR structure calculation with CYANA. *Methods Mol. Biol.* 278, 353–378.
- (54) Cornilescu, G., Delaglio, F., and Bax, A. (1999) Protein backbone angle restraints from searching a database for chemical shift and sequence homology. *J. Biomol. NMR* 13, 289–302.
- (55) Linge, J. P., Habeck, M., Rieping, W., and Nilges, M. (2003) ARIA: Automated NOE assignment and NMR structure calculation. *Bioinformatics* 19, 315–316.
- (56) Laskowski, R. A., Rullmann, J. A., MacArthur, M. W., Kaptein, R., and Thornton, J. M. (1996) AQUA and PROCHECK-NMR: Programs for checking the quality of protein structures solved by NMR. *J. Biomol. NMR* 8, 477–486.
- (57) Humphrey, W., Dalke, A., and Schulten, K. (1996) VMD: Visual molecular dynamics. *J. Mol. Graphics* 14, 27–38.
- (58) Schrodinger, LLC (2010) *The PyMOL Molecular Graphics System*, version 1.3r1.
- (59) Durney, M. A., Birrane, G., Anklin, C., Soni, A., and Ladas, J. A. (2009) Solution structure of the human Tax-interacting protein-1. *J. Biomol. NMR* 45, 329–334.
- (60) Schultz, J., Hoffmuller, U., Krause, G., Ashurst, J., Macias, M. J., Schmieder, P., Schneider-Mergener, J., and Oschkinat, H. (1998) Specific interactions between the syntrophin PDZ domain and voltage-gated sodium channels. *Nat. Struct. Biol.* 5, 19–24.

(61) Yan, X., Zhou, H., Zhang, J., Shi, C., Xie, X., Wu, Y., Tian, C., Shen, Y., and Long, J. (2009) Molecular mechanism of inward rectifier potassium channel 2.3 regulation by tax-interacting protein-1. *J. Mol. Biol.* 392, 967–976.

(62) Lipari, G., and Szabo, A. (1980) Effect of librational motion on fluorescence depolarization and nuclear magnetic resonance relaxation in macromolecules and membranes. *Biophys. J.* 30, 489–506.